PHYSICAL REVIEW B VOLUME 28, NUMBER 9 1 NOVEMBER 1983

Study of new $4f^7$ levels of Eu^{2+} in CaF_2 and SrF_2 using two-photon absorption spectroscopy

M. C. Downer* and C. D. Cordero-Montalvo†
Division of Applied Sciences, Harvard University, Cambridge, Massachusetts 02138

H. Crosswhite
Chemistry Divison, Argonne National Laboratory, Argonne, Illinois 60439
(Received 22 July 1983)

Two-photon dye-laser excitation is used to observe numerous sharp $4f^7$ levels of Eu^{2+} in CaF_2 and SrF_2 which are overlapped by the $4f^6 5d$ band, and thus inaccessible to single-photon spectroscopy. $4f^7$ excited states belonging to the ^6I and ^6D groups have been identified for the first time. Energy-level calculations are presented which confirm the f^7-level assignments and determine free-ion and crystal-field parameters for both host lattices. Measurements of the relative intensities and polarization dependence of the $f^7 \rightarrow f^7$ transitions confirm the existence of third- and fourth-order contributions to the two-photon intensities which have been postulated in recent analyses of the two-photon spectrum of the isoelectronic Gd^{3+} ion. In some cases ($^8S_{7/2} \rightarrow {}^6P_{7/2,5/2}, {}^6D_{7/2}$), however, these higher-order contributions are weaker than expected. It is shown that by relaxing the closure approximation in summing over the intermediate states, the agreement with the data is improved.

I. INTRODUCTION

We recently presented a comprehensive report and analysis[1] (subsequently referred to as I) of our observations[2–4] of numerous direct two-photon transitions between levels of the $4f^7$ configuration of Gd^{3+} in LaF_3 and in aqueous solution. The observations revealed widespread and severe discrepancies with the angular momentum selection rules ($\Delta L, \Delta J \leq 2$), relative intensities, and polarization dependence predicted by a standard second-order theory[5] of two-photon absorption (TPA). Subsequent analysis,[1] however, demonstrated that the discrepancies could be explained in quantitative detail by expanding the theory of TPA to include third- and fourth-order contributions which take into account spin-orbit[6] and crystal-field[3] interactions among levels of the excited $4f^6 5d$ configuration, which serve as intermediate states.

In the present work we use two-photon spectroscopy to study the $4f^7$ levels of the isoelectronic Eu^{2+} ion in the cubic crystals CaF_2 and SrF_2. Experimental details of the Eu^{2+} samples are described in Sec. II. Because the excited $4f^6 5d$ configuration lies at much lower energy in the divalent ion, it completely overlaps even the lowest sharp $4f^7$ excited states, which lie in the near ultraviolet. Consequently, only the intense broad bands arising from electric dipole allowed $4f^7 \rightarrow 4f^6 5d$ transitions can be seen in the single-photon absorption spectrum of these crystals.[7] With TPA, however, the broad bands are suppressed by the parity selection rule, allowing the sharp $4f^7$ levels to be observed. Fritzler and Schaak[8,9] first demonstrated this possibility by observing the $^6P_{7/2,5/2}$ levels of $4f^7$ in Eu^{2+}:CaF_2,SrF_2. These two levels had been observed earlier in the one-photon spectrum of Eu^{2+} in $KMgF_2$,[10] alkaline-earth sulfates,[11] and ternary alkaline-earth aluminum fluorides,[12] where they lie just below the onset of the $4f^6 5d$ absorption band edge. In the present study we have also observed the higher excited states in CaF_2 and SrF_2 belonging to the ^6I and ^6D groups for the first time. In Sec. III the evidence for identifying the new spectral lines as $4f^7$ levels is presented. Energy-level calculations which confirm these assignments are the subject of Sec. IV.

Because the separation E_{df} of the single-photon energy from the average energy of the intermediate $4f^6 5d$ states is roughly a factor of 3 smaller in Eu^{2+} than in Gd^{3+}, an increase in the absolute two-photon line strengths is expected and observed. Moreover, since the nth-order contribution to TPA scales as $E_{df}^{2(n-1)}$, we expect transitions which owe their strength primarily to third- and fourth-order contributions to increase considerably more in intensity than those dominated by the second-order contribution. Measurements of the relative intensities and polarization dependence of the $^8S_{7/2} \rightarrow {}^6P_J, {}^6I_J$ and ^6D_J two-photon transitions, described in Sec. III, bear out this expectation in some cases ($^8S_{7/2} \rightarrow {}^6I_J$), but not in others ($^8S_{7/2} \rightarrow {}^6P_{7/2,5/2}, {}^6D_{7/2}$). In the analysis of the two-photon line strengths, presented in Sec. V, it is argued that this discrepancy may result in part from a much greater relative spread of the energy denominators for the various intermediate states. The closure approximation conventionally used to simplify the sum over intermediate states thus becomes questionable. When the closure approximation is relaxed by introducing term-dependent energy denominators, the agreement between predicted and observed intensities improves for the $^6P_{7/2,5/2}, {}^6D_{7/2}$ lines, although a significant discrepancy remains for $^6P_{7/2}$. The Eu^{2+} results thus confirm the general expectations of the theory developed to explain the earlier Gd^{3+} data,[1] although the quantitative agreement is less satisfactory.

II. EXPERIMENT

The experimental apparatus and procedure have been fully described in I and elsewhere,[3,4] so only details of the Eu^{2+} samples will be described here. The beam from a nitrogen laser-pumped dye laser propagated along the [110] axis of the CaF_2 and SrF_2 crystals, which were mounted on the cold finger of a cryostat capable of being cooled to liquid-nitrogen or -helium temperatures. The samples were single crystals approximately 0.5 cm^3 in size, and were obtained from Optovac, Inc. The following polarizations of the excitation beam were examined: $\vec{E}||[111]$, $\vec{E}||[100]$, and circular polarization. Measurements at these three polarizations are sufficient to characterize completely the anisotropy of TPA.[13–15] The TPA intensity was an extremum at the two linear polarization directions.

Eu^{2+} enters CaF_2 and SrF_2 in a single type of substitution site possessing cubic (O_h) symmetry. A 0.03-mol % Eu^{2+}:CaF_2 sample and two SrF_2 samples of 0.03 and 0.1 mol % were studied. Because of the possible presence of Eu^{3+} at interstitial sites,[16] which could give rise to spurious spectral lines, attempts were made to estimate the Eu^{3+} content by exciting the $^7F_0 \rightarrow {}^5D_2$ Eu^{3+} absorption line with the dye laser tuned to about 4655 Å. Subsequent fluorescence from $^5D_{0,1} \rightarrow {}^7F_J$ relaxation was monitored with a filtered photomultiplier tube (PMT). No Eu^{3+} whatsoever was detectable in the CaF_2 sample, although concentrations smaller than 10^{-4} mol % should have been detectable. Nevertheless, the crystal was annealed to eliminate any trace Eu^{3+}. Weak Eu^{3+} absorption was detected in both SrF_2 samples. Annealing in a reducing atmosphere[16] lowered, but did not eliminate, the Eu^{3+} concentration. Nevertheless, the TPA spectral lines observed in the SrF_2 samples corresponded closely to those seen in CaF_2, indicating that Eu^{3+} was not the source of them.

The two-photon excitation spectrum of all three samples was recorded over the entire range extending from $2\nu_{laser}=27\,500$ to $36\,500$ cm^{-1}. Violet fluorescence from one-photon relaxation back to the $^8S_{7/2}$ ground state was collected at right angles to the excitation beam with a suitably filtered PMT. No fluorescence was observed directly from the $4f^7$ excited states, which are shown in Fig. 1. Instead the excitation is transferred to the overlapping $4f^65d$ band via odd-parity lattice vibrations, followed by fluorescence at 4130 Å in CaF_2 and 4010 Å in SrF_2. Fluorescence yield is essentially unity because of the large energy gap (24 000 cm^{-1}) separating the lowest excited states from the ground state. Consequently, fluorescence intensity is proportional to TPA.

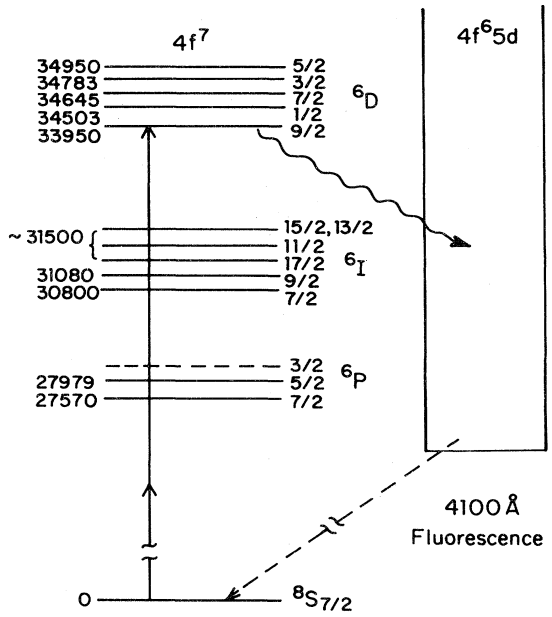

FIG. 1. Energy-level diagram for Eu^{2+}:CaF_2 showing two-photon excitation of $^6D_{9/2}$ and subsequent nonradiative and radiative relaxation. Left-hand column gives average energy of each J multiplet in cm^{-1}. Note the overlap of $4f^65d$ and $4f^7$ levels.

III. EXPERIMENTAL RESULTS

A. Observation and identification of $4f^7$ levels

Figures 2–5 show experimental two-photon excitation recordings of selected ^6P, ^6I, and ^6D lines in Eu^{2+}:CaF_2,SrF_2 at 80 K. Recordings of other observed lines have been included in Ref. 4. The vertical scale of Figs. 2–5 indicates the normalized TPA intensity in arbitrary units on the same internally consistent scale. The slowly varying background TPA signal from $4f^7 \rightarrow 4f^65d$ absorption, which was observed throughout the experimental tuning range, is clearly evident beneath the sharp peaks in these figures. The sloping background beneath the ^6D lines in Fig. 5 is the rising edge of the $4f^5(^7F)^5d\,(E_g)$ peak.

The sharp lines were concentrated in three groups, which fell consistently at about 85% of the energy of the corresponding ^6P, ^6I, and ^6D lines in the isoelectronic Gd^{3+} ion, consistent with a 15—20 % reduction in the Coulomb and spin-orbit parameters for the divalent ion. A nearly uniform blue shift of 100 cm^{-1} of the SrF_2 lines from the CaF_2 line positions observed by Fritzler[9] for the ^6P lines was observed in the present spectrum also for the higher-energy lines, confirming that they are indeed f^7 levels from the same ion. Similar weak shifts are characteristic of the $4f^7$ levels[17] of Gd^{3+} as well as $4f^N$ levels of other rare earths in different host crystals.[18] The red shift of 700 to 800 cm^{-1} of the ^6P and ^6I lines from their positions in the free Eu^{2+} ion[19] is also typical of $4f^N$ levels. By contrast, the $4f^65d$ absorption edge is 10 000 cm^{-1} lower in the crystals than in the free ion, and 700 cm^{-1} higher in SrF_2 than in CaF_2. The weak temperature dependence of the observed linewidths is a further trademark of $4f^N$ lines. The stronger lines were observed easily even at room temperature.

The close correspondence between the line positions and relative line intensities in all three samples, as well as the observed proportionality of line intensities to known Eu^{2+}

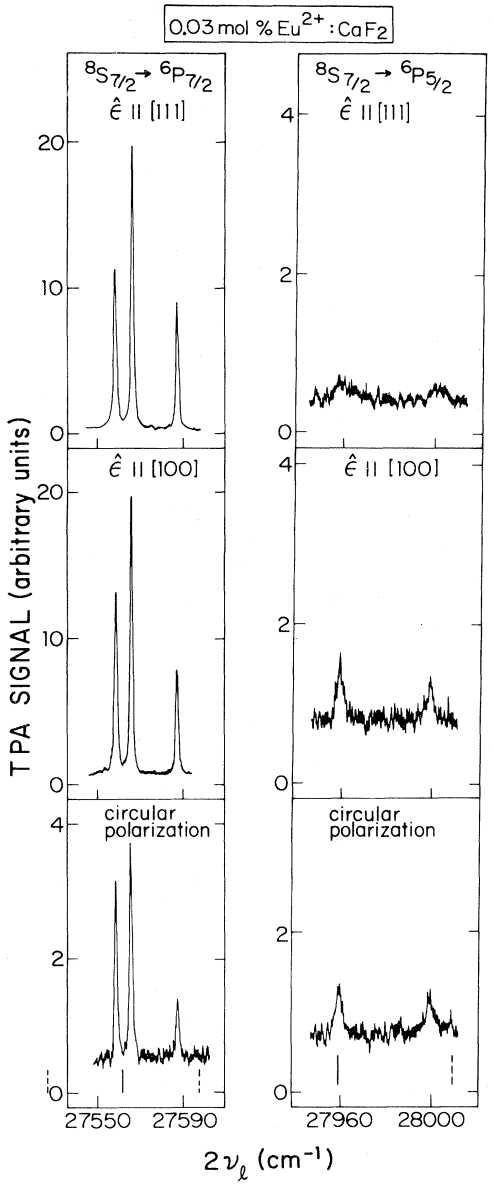

FIG. 2. Experimental two-photon excitation recordings of $^6P_{7/2,5/2}$ in Eu^{2+}:CaF_2 at 80 K for three polarizations of the excitation beam, showing clearly resolved Stark components and a substantially weaker $^6P_{7/2}$ intensity for circular polarization. Vertical lines show calculated Stark-component positions. Dashed lines denote single Kramers doublets; solid lines denote two degenerate Kramers doublets.

concentration, served to rule out further the possibility that the sharp lines arose from trace impurities other than Eu^{2+}. In addition, spectral analysis of the fluorescence following two-photon excitation of lines in all three groups consistently revealed only the single wavelengths 4130 Å in CaF_2 and 4010 Å in SrF_2, which are the characteristic Eu^{2+} fluorescence frequencies in these crystals.

We have also observed the $^6P_{7/2}$ multiplet in 0.1 mol % Eu^{2+}:BaF_2, blue shifted 80 cm^{-1} from its position in SrF_2, and with three Stark components characteristic of a cubic substitution site. In sharp contrast to the other crystals, however, the characteristic violet fluorescence was not observed. Instead the excitation evidently transferred to neighboring Eu^{3+} ions also present in the crystal, which then fluoresced weakly in the red. The nature of this energy-transfer mechanism is being investigated further.

B. Linewidths and intensities of $4f^7$ levels

The new ^6I and ^6D lines were, on the whole, considerably broader at a given temperature than the lower-energy ^6P lines, as can be seen by comparing Figs. 3–5 to Fig. 2. The ^6I and ^6D lines narrowed slightly upon cooling to liquid-helium temperature, but remained much broader than the ^6P lines. Consequently, crystal-field splitting of these levels was not completely resolved. We believe these lines are broader because the overlapping $4f^6 5d$ band changes from octet at lower energies to sextet at higher energies in accordance with Hund's rule. Since the vibrational interaction does not flip electron spins, the higher f^7 levels vibrationally couple more strongly to neighboring sextet levels of $4f^6 5d$ than the lower levels to neighboring octets. In the free-ion spectrum[19] of Eu^{2+} the lowest sextets of $4f^6 5d$ occur at 41 000 cm^{-1}. Taking into account the lowering of $4f^6 5d$ by 10 000 cm^{-1} in the crystals, we estimate the onset of the sextets to be about 31 000 cm^{-1}, precisely the position of the ^6I lines (see Fig. 1). The sextets continue upward well beyond the position of the ^6D lines. The ^6P lines, by contrast, must be surrounded entirely by octets.

The relative intensities of the two-photon transitions were measured and normalized using the procedure described in I. The bar graph in Fig. 6 presents the normalized two-photon absorption line strengths for Eu^{2+}:CaF_2 on an arbitrary logarithmic scale. Each vertical bar represents the intensity for a particular polarization of the excitation beam of a J multiplet integrated over all crystal-field components. In some cases, because of inadequate resolution or strong mixing of the J values of some closely spaced lines, the total line strength of two or more J multiplets has been represented by a single bar. The horizontal lines in Fig. 6 denote relative intensities predicted by the second-order theory of Axe,[5] where the best fit has been made to the four transition intensities, $^8S_{7/2} \rightarrow {}^6P_{5/2}, {}^6D_{9/2,3/2,5/2}$. Analysis of analogous data[1] for Gd^{3+} showed that only these four transitions were correctly explained by a second-order theory. Their relative intensities again agree with second-order predictions in Eu^{2+}:CaF_2. The weak $^6P_{3/2}$ line could not be observed above the background absorption.

The remaining transitions show enormous discrepancies with the second-order theory which qualitatively resemble the discrepancies observed for Gd^{3+}. In particular, the ^6I_J lines are many orders of magnitude stronger than the second-order theory predictions, which fall below the scale of Fig. 6. In fact, as in Gd^{3+}, $^8S_{7/2} \rightarrow {}^6I_{13/2,15/2,17/2}$ should have zero intensity since the selection rule $\Delta J \leq 2$ is violated. In addition, the $^6P_{7/2}$ line displays the unique anomalous enhancement for linear polarization which was

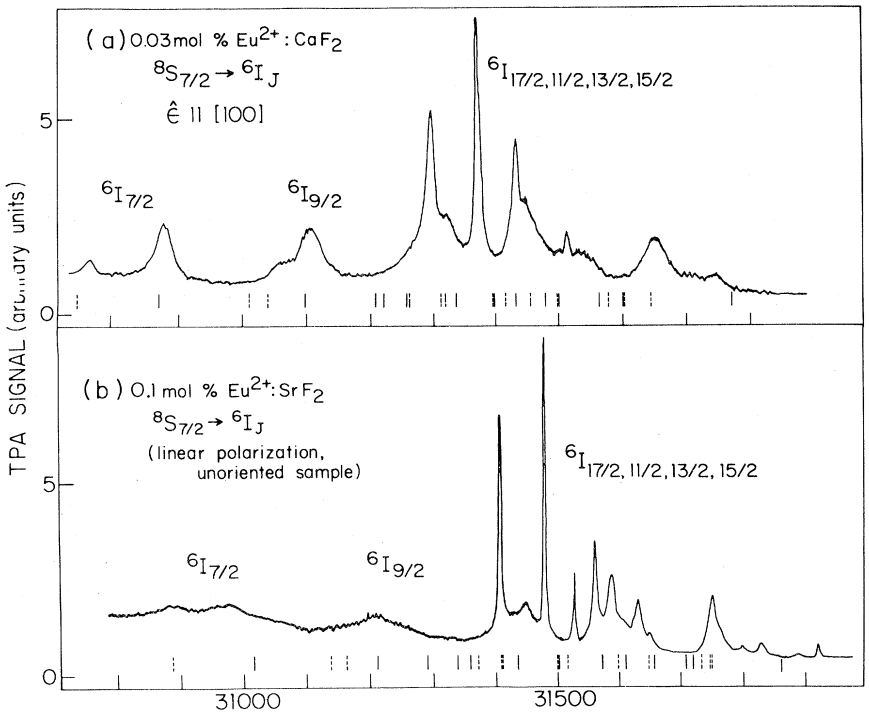

FIG. 3. Experimental two-photon excitation recordings of the ^6I_J group in (a) $Eu^{2+}:CaF_2$ and (b) $Eu^{2+}:SrF_2$. Note the close correspondence between the levels in the two crystals and the blue shift of approximately 100 cm^{-1} in SrF_2. The vertical scale shows the TPA signal normalized to a standard laser intensity and dopant concentration. Vertical lines show calculated Stark-component positions, with notation as in Fig. 2.

observed in Gd^{3+}, and which directly contradicts the Axe theory. Finally, $^8S_{7/2} \rightarrow {}^6D_{1/2}$, which also violates $\Delta J \leq 2$, shows a substantial observable intensity.

In addition to these similarities, however, the Eu^{2+} data differ in several important ways from the corresponding Gd^{3+} data. Most notably, there are significant differences in the relative intensities of some of the lines. The ^6I_J lines, relative to $^6P_{5/}$ and ^6D_J, are an order of magnitude stronger than in Gd^{+}. The anisotropy of these lines is also different and less pronounced than in $Gd^{3+}:LaF_3$. The ratios $S(^6P_{7/2}$,linear$)/S(^6P_{7/2}$,circular) and $S(^6P_{7/2})/S(^6P_{5/2})$, on the other hand, are roughly a factor of 2 smaller in Eu^{2+} than in Gd^{3+}. Our data on these latter intensities agree with those of Fritzler[9] within experimental error. The cross section for $^6D_{1/2}$ is nearly isotropic, in contrast to its strong anisotropy in $Gd^{3+}:LaF_3$. In addition, it is somewhat stronger with respect to the neighboring $^6D_{7/2}$. Finally, most transitions (excepting $^8S_{7/2} \rightarrow {}^6P_{7/2}, {}^6D_{1/2,7/2}$) show some experimentally reproducible anisotropy, including four transitions ($^8S_{7/2} \rightarrow {}^6P_{5/2}, {}^6D_{9/2,3/2,5/2}$) which were isotropic in $Gd^{3+}:LaF_3$. Stronger crystal-field mixing of the $4f^7$ levels is probably responsible for the anisotropy of these latter transitions. This J mixing has not been included in arriving at the second-order theoretical predictions shown in Fig. 6.

IV. ENERGY-LEVEL CALCULATIONS

Energy-level calculations for the $4f^7$ configuration in a cubic substitution site have been performed earlier for Gd^{3+} in CaF_2 (Ref. 20) and for Eu^{2+} in CaF_2 and SrF_2.[9] In both of these calculations experimental energy levels were available only for $^6P_{7/2}$ and $^6P_{5/2}$. The chief advantage of the present calculation is the much larger number of observed levels which can be incorporated into the fitting program. Our analysis employs fitting programs developed at Argonne National Laboratory, which have been used previously in extensive calculations of $R^{3+}:LaCl_3$ and $R^{3+}:LaF_3$ energy levels,[21] where R represents rare earth.

A. Center-of-gravity-calculation

As a preliminary calculation, the observed centers of gravity of those J multiplets ($^6P_{7/2,5/2}, {}^6I_{7/2,9/2}, {}^6D_{9/2,1/2,7/2,3/2}$) which in our opinion could be assigned unambiguously were fitted without the crystal-field interaction in order to obtain free-ion eigenfunctions. All Russell-Saunders multiplets allowed in f^7 were used as a basis. An accurate set of intermediate-coupling free-ion eigenfunctions is an essential prerequisite to crystal-field calculations in the half-filled f^7 shell, since diagonal matrix elements $(^{2S+1}L_J||U^{(k)}||^{2S+1}L_J)$, and therefore first-

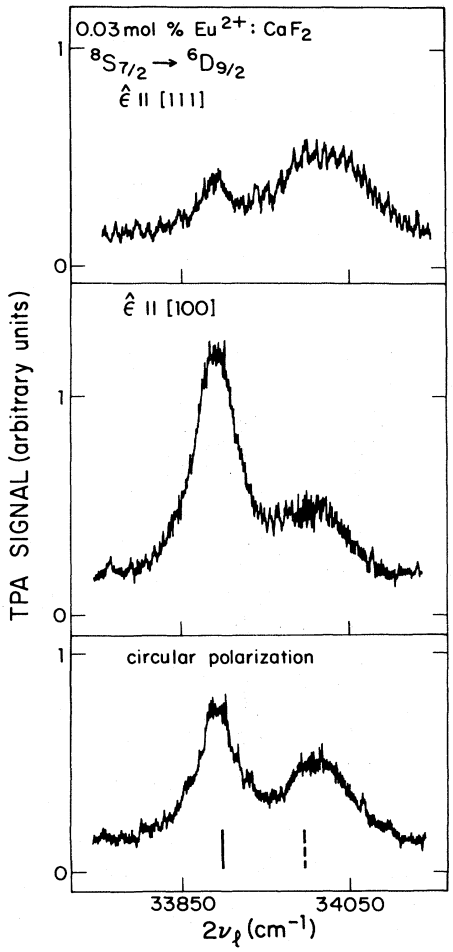

FIG. 4. Experimental two-photon excitation recording of $^6D_{9/2}$ in Eu^{2+}:CaF_2 at 80 K. Vertical lines are calculated Stark-component positions as in Fig. 2. A third component was calculated to fall at 33 659 cm^{-1}, but was not observed.

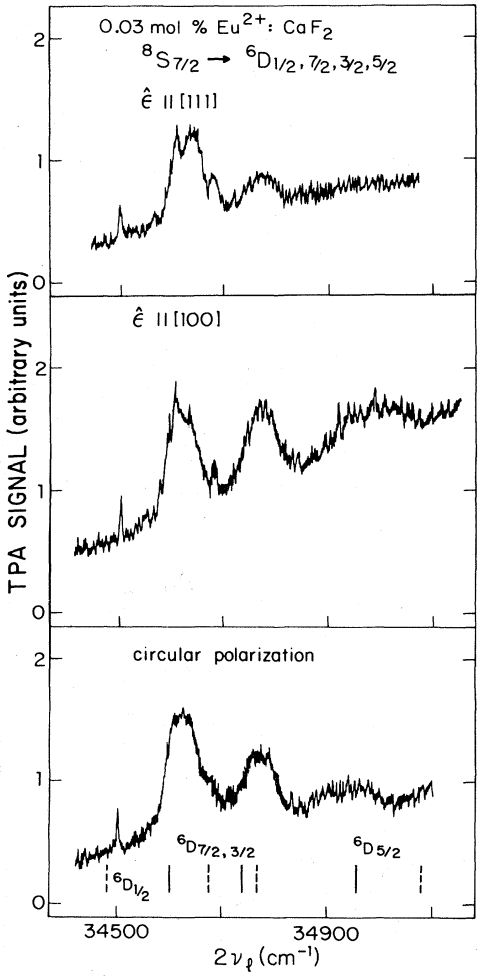

FIG. 5. Experimental two-photon excitation recordings of $^6D_{1/2,7/2,3/2,5/2}$ in Eu^{2+}:CaF_2, comparing observed peaks with calculated level positions (vertical lines as in Fig. 2). The sloping background arises from $4f^7 \rightarrow 4f^6 4d$ two-photon absorption.

order crystal-field splitting, vanish in the Russell-Saunders limit.

The free-ion Hamiltonian has the form

$$H = H_0 + H_e + H_{so} + H_{conf} + H_{soo} \ . \quad (1)$$

H_0 includes the electron kinetic energy and central field potential. H_e is the interelectronic Coulomb repulsion among $4f$ electrons, which is parametrized in terms of the Slater integrals[22] $F^{0,2,4,6}$, while the H_{so} is the spin-orbit interaction of the $4f$ electrons. H_{conf} denotes an effective Hamiltonian resulting from the interaction of $4f^7$ with other odd-parity configurations, and is parametrized by three two-body integrals,[23] α, β, and γ, and six three-body integrals[24] $T^{2,3,4,6,7,8}$. The interaction of $4f^7$ with excited configurations through the combined action of electrostatic and spin-orbit interactions[25,26] results in an effective term dependence of the spin-orbit coupling constant ζ_f, an effect which is parametrized by the three additional quantities $P_{2,4,6}$. The final operator in (1) denotes relativistic corrections, specifically spin-other-orbit interactions, which are expressed in terms of the Marvin's integrals[24,26] $M^{0,2,4}$.

Altogether 20 parameters are involved in calculating the free-ion energy levels. The parameters F^2, ζ_f, and γ were freely varied in obtaining the fit. F^4 and F^6 were chosen to stand in the approximate ratios $2F^6 = 1.5F^4 = F^2$, then held fixed through the calculation. The remaining parameters were set equal to values which had been determined[21] for the isoelectric Gd^{3+} ion, and also held fixed. A least-squares fit yielded a mean-square deviation σ of about 50 cm^{-1} from the observed centers of gravity, and free-ion eigenfunctions were extracted which served as a basis for the crystal-field calculation.

B. Crystal-field calculation

The crystal-field (CF) Hamiltonian in O_h symmetry has the form

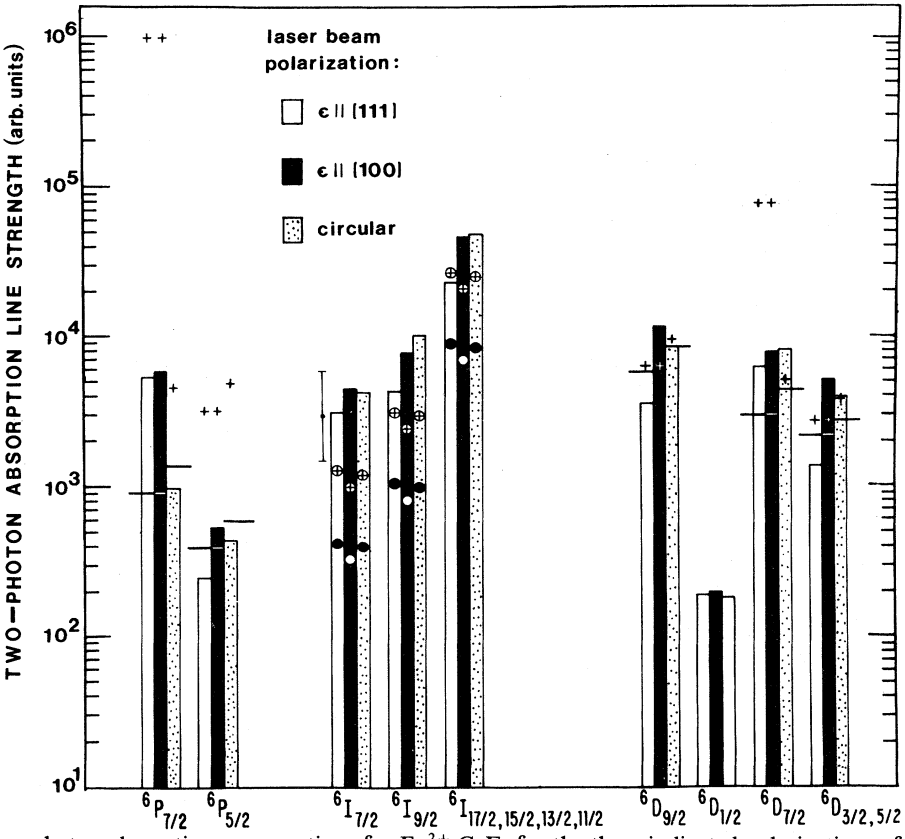

FIG. 6. Relative two-photon absorption cross sections for Eu^{2+}:CaF_2 for the three indicated polarizations of the excitation beam. Horizontal lines denote predictions of the second-order theory of TPA. Crosses denote line strengths predicted by including third-order terms involving the spin-orbit interaction, circles (open and solid) by including third-order terms involving the crystal-field interaction, and circled crosses by including fourth-order terms. The closure approximation has been used in arriving at all theoretical values shown.

$$H_{\mathrm{CF}}=B_0^{(4)}[C_0^{(4)}+(\tfrac{5}{14})^{1/2}(C_4^{(4)}+C_{-4}^{(4)})] +B_0^{(6)}[C_0^{(6)}-(\tfrac{7}{2})^{1/2}(C_4^{(6)}+C_{-4}^{(6)})]\,, \quad (2)$$

where $C_q^{(k)}$ are tensor operators proportional to spherical harmonics Y_{kq} and $B_q^{(k)}$ are empirical coefficients determined by the charge distribution of the surrounding lattice and by radial integrals of $4f$ electrons. The matrix of H_{CF} breaks down into two submatrices corresponding to the two values $\mu=\frac{1}{2}$ and $\frac{3}{2}$ of the crystal quantum number of Hellwege.[27] Each of these submatrices breaks down further into two equivalent submatrices because of Kramers degeneracy, leaving two independent submatrices to be diagonalized. Because it was not practical at this stage of the calculation to use the full f^7 basis set, we adopted the method described in Ref. 20(b), whereby a truncated intermediate-coupling basis set was used which gave a full representation of all the original set, at the cost only of removing distant states whose perturbations through the crystal fields were negligible. The resulting crystal-field submatrices were of rank 163.

In several trial crystal-field calculations, the observed components of ^6P_J, ^6D_J, and $^6I_{7/2,9/2}$ were included in the fit, and the crystal-field parameters $B_0^{(4)}$ and $B_0^{(6)}$, along with F^2, ζ_f, and E_{av} (average energy of f^7 configuration), were freely varied. Significant improvements in the fit were then found to result from allowing selected additional parameters, in particular F^4, F^6, and P_2, to vary as well. Most of the higher ^6I levels were granted level assignments as they became clear from preliminary fitting runs, then included in the final fit. Care was exercised to maintain identical assignments for levels in CaF_2 and SrF_2 which, judging from their spacing from adjacent levels and relative intensities, appeared to correspond to one another.

C. Results and discussion

The results of the final fit are shown in Table I. The positions of many calculated levels have also been indicated in Figs. 2–5. The experimental positions listed were measured at 80 K by monitoring the laser frequency with a calibrated 1-m spectrometer. Accuracies vary from ± 1 cm^{-1} for the sharpest lines to ± 10 cm^{-1} for the broadest lines.

The final values of the variable parameters determined by the fit are listed at the bottom of Table I.

TABLE I. Observed and calculated Stark-component energes in cm^{-1} of the ^6P, ^6I, ^6D multiplets for Eu^{2+} in CaF_2 and SrF_2.

	Eu^{2+}:CaF_2			Eu^{2+}:SrF_2		
Term	Obs.	Calc.[a]	Composition[b]	Obs.	Calc.[c]	Composition[b]
$^6P_{7/2}$	27 558	27 527	−0.74(3,0)−0.63(3,−3)	27 654	27 608	−0.75(3,0)−0.63(3,−3)
	27 564	27 562	0.74(3,−3)−0.63(3,0)	27 658	27 650	0.75(3,−3)−0.63(3,0)
			−0.84(3,1)−0.49(3,−2)			−0.85(3,1)−0.49(3,−2)
	27 588	26 598	−0.84(3,−2)+0.49(3,1)	27 672	27 703	−0.85(3,−2)+0.49(3,1)
$^6P_{5/2}$	27 959	27 961	−0.97(2,0)+0.11(8,4)	28 066	27 059	−0.98(2,0)+0.09(8,4)
			−0.88(2,−2)−0.40(2,1)			−0.89(2,−2)−0.40(2,1)
	27 999	28 011	0.88(2,1)−0.39(2,−2)	28 098	28 132	0.88(2,1)−0.40(2,−2)
$^6P_{3/2}$		28 424	−0.96(1,0)+0.12(6,−3)		28 540	−0.97(1,0)+0.10(6,−3)
			0.96(1,1)+0.13(7,5)			0.97(1,1)+0.10(7,5)
$^6I_{7/2}$	30 760	30 747	0.74(3,0)+0.62(3,−3)	30 887	30 887	0.73(3,0)+0.62(3,−3)
	30 880	30 872	−0.71(3,−3)+0.60(3,0)	31 000	31 016	−0.71(3,−3)+0.60(3,0)
			−0.81(3,1)−0.47(3,−2)			−0.80(3,1)−0.46(3,−2)
		31 010	−0.82(3,−2)+0.47(3,1)		31 163	−0.82(3,−2)+0.47(3,1)
$^6I_{9/2}$	31 057	31 039	−0.68(4,0)−0.55(4,4)		31 139	−0.55(4,0)−0.53(4,4)
	31 107	31 097	−0.62(4,4)+0.51(4,0)	31 210	31 212	−0.57(4,4)+0.47(4,0)
			0.59(4,−2)+0.55(4,1)			0.54(4,−2)+0.50(4,1)
		31 221	−0.75(4,−3)−0.28(8,4)		31 359	−0.58(8,4)−0.54(4,−3)
			0.69(4,−2)−0.38(4,1)			0.49(8,−6)+0.43(4,−2)
$^6I_{17/2,11/2,13/2,15/2}$		31 208	0.60(8,8)−0.32(8,−3)		31 291	0.66(8,−7)+0.45(8,−3)
			0.61(8,1)+0.48(4,1)			−0.54(8,1)+0.48(8,−2)
		31 256	−0.70(8,−7)−0.41(8,−3)		31 339	0.56(8,8)−0.46(8,0)
			−0.71(8,−2)−0.42(8,−6)			−0.53(8,−2)−0.42(8,1)
		31 260	0.55(8,0)+0.55(8,−3)		31 372	0.71(8,−3)−0.41(8,−7)
	31 296	31 312	−0.58(5,1)+0.48(5,5)	31 407	31 409	0.45(5,1)+0.40(8,5)
		31 318	−0.50(8,4)−0.45(8,−7)		31 411	−0.57(8,0)−0.41(8,8)
	31 318	31 334	0.51(5,0)+0.42(6,0)	31 450	31 436	0.72(4,−3)−0.31(6,0)
			0.45(5,5)+0.37(8,1)			−0.54(4,1)+0.50(4,−2)
	31 371	31 394	−0.68(7,0)−0.55(7,−7)	31 479	31 500	−0.60(7,0)−0.49(7,−7)
		31 397	−0.54(8,4)+0.44(5,0)		31 502	0.67(5,0)−0.36(8,4)
			−0.50(8,−6)−0.40(8,5)			0.60(5,5)+0.36(8,1)
		31 416	−0.76(8,5)+0.34(8,−6)	31 526	31 517	−0.67(8,5)+0.36(5,1)
	31 433	31 432	−0.51(7,−7)+0.43(7,0)	31 561	31 572	−0.49(7,−7)+0.43(6,0)
			−0.57(7,1)+0.37(6,−6)			0.51(7,1)−0.41(6,−6)
	31 446	31 455	0.74(5,−3)+0.33(5,4)	31 590	31 598	0.77(5,−3)+0.34(5,4)
	31 485	31 479	0.50(6,0)+0.44(5,4)	31 610	31 611	0.52(6,0)−0.43(7,−7)
			−0.50(6,−6)−0.45(5,−2)			0.50(6,−6)+0.42(7,1)
	31 513	31 499	0.46(6,1)−0.39(6,−6)	31 632	31 648	0.54(6,1)−0.45(6,−6)
		31 500	0.62(5,4)+0.34(7,−7)	31 647	31 657	0.78(5,4)−0.33(5,−3)
			0.53(5,−2)−0.42(5,1)			0.68(5,−2)−0.51(5,1)
	31 540	31 565	0.78(7,4)+0.42(6,−3)		31 709	0.71(7,4)−0.57(7,−3)
			0.48(7,−6)−0.44(7,−2)			0.65(7,−6)−0.59(7,−2)
	31 653	31 578	−0.70(6,−2)+0.62(6,5)	31 749	31 733	−0.57(6,−2)+0.43(7,−6)
		31 601	−0.79(7,−3)−0.26(6,−3)		31 720	−0.67(7,−3)−0.44(6,−3)
			−0.53(7,5)−0.51(7,−6)			−0.68(7,5)−0.42(6,5)
		31 603	−0.80(6,4)−0.42(6,−3)	31 766	31 746	−0.79(6,4)−0.41(6,−3)
	31 710	31 645	−0.49(7,−6)−0.45(7,−2)	31 800	31 750	−0.51(6,5)+0.40(6,−2)
	31 748	31 771	−0.51(6,−3)+0.50(7,4)	31 828	31 862	−0.55(6,−3)+0.48(7,4)
			0.60(7,5)−0.46(6,5)			0.57(7,5)−0.49(6,5)

Eu^{2+}:CaF_2,SrF_2 differ from Gd^{3+}:CaF_2 (Ref. 20) principally by having smaller Coulomb and spin-orbit interactions and larger crystal-field interactions, all of which result from the larger ionic radius of the divalent ion. The present fit required somewhat larger crystal-field parameters than the earlier calculation of Fritzler,[9] which was based only on the $^6P_{7/2,5/2}$ levels, although the Coulomb and spin-orbit parameters were similar to those deter-

TABLE I. (*Continued.*)

Term	Eu^{2+}:CaF_2 Obs.	Calc.[a]	Composition[b]	Eu^{2+}:SrF_2 Obs.	Calc.[c]	Composition[b]
$^6D_{9/2}$		33 659	$-0.93(4,-3)+0.29(2,4)$		33 644	$-0.92(4,-3)+0.28(4,0)$
			$0.86(4,-2)-0.48(4,1)$			$0.83(4,-2)-0.48(4,1)$
	33 890	33 899	$-0.78(4,4)+0.57(4,0)$	33 990	33 996	$-0.78(4,4)+0.57(4,0)$
			$-0.86(4,1)-0.49(4,-2)$			$-0.84(4,1)-0.51(4,-2)$
	34 010	33 997	$-0.74(4,0)-0.59(4,4)$	34 115	34 122	$-0.73(4,0)-0.58(4,4)$
$^6D_{1/2}$	34 503	34 480	$-0.90(0,0)+0.29(3,0)$		34 533	$-0.86(0,0)+0.36(3,0)$
$^6D_{7/2,3/2,5/2}$	34 620	34 600	$0.63(1,0)-0.57(3,-3)$	34 650	34 655	$0.67(1,0)-0.53(3,-3)$
			$-0.64(3,1)+0.63(1,1)$			$-0.67(1,1)+0.60(3,1)$
	34 685	34 676	$-0.83(3,-2)+0.48(3,1)$	34 740	34 751	$-0.82(3,-2)+0.47(3,1)$
		34 740	$-0.73(2,0)+0.56(1,0)$	34 770	34 795	$-0.79(2,0)+0.46(1,0)$
	34 785		$0.67(2,-2)+0.56(1,1)$			$0.72(2,-2)+0.46(1,1)$
		34 769	$-0.69(3,0)-0.59(3,-3)$	34 860	34 847	$-0.65(3,0)-0.55(3,-3)$
	34 950	34 955	$-0.65(2,0)-0.52(1,0)$		35 055	$-0.58(2,0)-0.55(1,0)$
			$-0.59(2,-2)+0.52(1,1)$			$-0.55(1,1)+0.53(2,-2)$
		35 078	$0.87(2,1)-0.39(2,-2)$		35 190	$0.86(2,1)-0.39(2,-2)$

[a]Variable parameters (cm^{-1}): $E_{av}=74\,668$, $F^2=70\,834$, $F^4=50\,902$, $F^6=38\,891$, $\zeta_f=1228$, $P_2=768$, $B_0^{(4)}=-3324$, $B_0^{(6)}=-1289$, 48 levels fitted, $\sigma=24.5$ cm^{-1}. Fixed parameters (cm^{-1}): $\alpha=18.6$, $\beta=-590$, $\gamma=1805$, $T^2=330$, $T^3=41.5$, $T^4=62$, $T^6=-295$, $T^7=360$, $T^8=310$, $M_0=2.66$, $M_2=1.54$, $M_4=1.01$, $P_4=450$, $P_6=300$.

[b]Two largest components of eigenfunction. Where two eigenfunctions are listed, degenerate levels occur in the $\mu=\frac{1}{2}$ and $\frac{3}{2}$ submatrices. Notation: The ordered pair (i_1,i_2) denotes a wave function with $J=\frac{1}{2}(2i_1+1)$ and $|M_J|=\frac{1}{2}(2|i_2|+1)$.

[c]Variable parameters (cm^{-1}): $E_{av}=75\,206$, $F^2=71\,937$, $F^4=50\,610$, $F^6=38\,967$, $\zeta_f=1233$, $P_2=619$, $B_0^{(4)}=-4874$, $B_0^{(6)}=-993$, 47 levels fitted, $\sigma=22.5$ cm^{-1}. Fixed parameters as in Ref. a.

mined in that study. Estimates of many-body effects, which were neglected in the previous study, have been included as fixed parameters, values of which are also given in Table I.

Table I indicates that the calculated average positions of the ^6P, ^6I, and ^6D groups correspond extremely well to the average positions of the three observed groups of lines. Furthermore, the calculated and observed centers of gravity of the individual terms agree to within 25 cm^{-1} in all cases, and considerably better in most cases, as shown by the comparison in Table II. This table shows the calculated centers of gravity after the crystal-field interaction has been included. The close agreement obtained constitutes strong evidence for the $4f^7$-level assignments.

Occasional complications were encountered in interpreting the finer details of the spectrum. Because of broad linewidths and close line spacing in the ^6I and ^6D groups, some observed lines appeared to comprise two or more Stark components. In addition, some calculated levels did not appear in the observed spectrum of either crystal, most notably the $^6P_{3/2}$ line, one Stark component each of $^6I_{7/2}$, $^6I_{9/2}$, and $^6D_{9/2}$, as well as the three lowest-energy components of $^6I_{17/2}$. Weak line intensities and/or broad linewidths may account for the failure of these expected lines to show up above the background TPA signal. Finally, two weak lines at 31 890 and 31 910 cm^{-1} observed in the spectrum of our 0.1-mol % Eu^{2+}:SrF_2 sample had no evident counterparts in Eu^{2+}:CaF_2. Attempts to assign these lines to calculated ^6I levels led to larger discrepancies elsewhere in the spectrum when the fit was run. We

TABLE II. Observed and calculated centers of gravity of the ^6P_J, ^6I_J, and ^6D_J multiplets in Eu^{2+}:CaF_2 and Eu^{2+}:SrF_2 in units of cm^{-1}.

Term	Eu^{2+}:CaF_2 Obs.	Calc.	(Obs.)−(Calc.)	Eu^{2+}:SrF_2 Obs.	Calc.	(Obs.)−(Calc.)
$^6P_{7/2}$	27 569	27 562	+7	27 661	27 653	+8
$^6P_{5/2}$	27 972	27 978	−6	28 077	28 083	−6
$^6I_{7/2}$	30 840	30 830[a]	+10	30 962	30 973[a]	−11
$^6I_{9/2}$	31 090	31 078[a]	+12	31 210	31 188[a]	+22
$^6I_{17/2,11/2,13/2,15/2}$	31 503	31 498[a]	+5	31 609	31 610[a]	−1
$^6D_{9/2}$	33 930	33 932[a]	−2	34 032	34 038[a]	−6
$^6D_{1/2}$	34 503	34 480	+23		34 533	
$^6D_{7/2,3/2,5/2}$	34 773	34 754[a]	+19	34 740	34 750[a]	−10

[a]Center of gravity of calculated Stark components excluding those which correspond to unobserved levels.

have therefore tentatively interpreted these lines as impurity levels or vibronic sidebands. All other lines, however, lend themselves to clear interpretation as zero-phonon $f^7 \rightarrow f^7$ transitions. Vibronic sidebands should be comparatively weak since the parent lines arise from parity-allowed electronic transitions. There was no evidence of sidebands accompanying the ^6P or ^6D lines.

The fit shown in Table I reproduces the magnitude of the observed crystal-field splitting of the $^6I_{7/2,9/2}$, ^6D_J multiplets in both crystals, as well as $^6P_{5/2}$ in CaF_2, to within 25 cm^{-1}. Furthermore, the observed $^6I_{17/2,11/2,13/2,15/2}$ lines fall consistently within 20 cm^{-1} of the calculated levels to which they have been assigned, with the exception of a few lines at the high-energy end of the group. A large discrepancy occurred, however, for $^6P_{7/2}$, where the observed total splitting was smaller by 41 and 77 cm^{-1}, respectively, in CaF_2 and SrF_2 than the calculated total splitting. Fritzler[9] noted earlier that the small $^6P_{7/2}$ splitting was inconsistent with the larger $^6P_{5/2}$ splitting. Our results indicate that it is also inconsistent with the splittings of the higher levels. The origin of the anomaly is not understood.

The mean-square deviations σ indicated in Table I for those Stark components which were fitted in Eu^{2+}:CaF_2 and Eu^{2+}:SrF_2 are comparable to σ values found in fitting most R^{3+}:$LaCl_3$ and R^{3+}:LaF_3 systems.[21] Nevertheless, improvements should be possible as more data become available on the $4f^N$ levels of other divalent lanthanides, since valuable clues often emerge from observing parameter trends across the lanthanide series.

V. ANALYSIS OF TWO-PHOTON INTENSITIES

A. Theoretical outline

We showed in I that a full account of the two-photon intensities of Gd^{3+}:LaF_3 required not only the standard second-order term

$$\sum_n \Delta_n^{-1}(g \mid \vec{E}\cdot\vec{D} \mid n)(n \mid \vec{E}\cdot\vec{D} \mid f) , \tag{3a}$$

but third- and fourth-order terms having the general forms

$$\sum_{m,n} \Delta_m^{-1}\Delta_n^{-1}(g \mid \vec{E}\cdot\vec{D} \mid m)(m \mid V \mid n)(n \mid \vec{E}\cdot\vec{D} \mid f) \tag{3b}$$

and

$$\sum_{l,m,n} \Delta_l^{-1}\Delta_m^{-1}\Delta_n^{-1}(g \mid \vec{E}\cdot\vec{D} \mid l)(l \mid V \mid m)(m \mid V' \mid n) \times (n \mid \vec{E}\cdot\vec{D} \mid f) , \tag{3c}$$

respectively. We now apply the same analysis to the Eu^{2+} data. V and V' denote some part of the unperturbed atomic Hamiltonian acting among the intermediate states l, m, and n, which belong to opposite-parity excited configurations. Δ_i is the energy of the intermediate state i above the single-photon energy. The line strength S_{TPA} of the transition from $g = \mid f^7\psi JM)$ to $f = \mid f^7\psi' J' M')$ is the square modulus of the sum of (3a)—(3c), summed over azimuthal quantum numbers M and M'.

B. $^8S_{7/2} \rightarrow {}^6I_J$: Third-order terms involving the crystal-field interaction and fourth-order terms

These transitions violate the second-order selection rules $\Delta L \leq 2$ and $\Delta S = 0$, and in three cases $\Delta J \leq 2$ as well. The use of intermediate-coupling initial- and final-state wave functions and the inclusion of intra-$4f^7$ crystal-field interactions cannot account for the observed intensities.[1,3] Crystal-field interactions within $4f^6 5d$, however, are 2 orders of magnitude stronger than within $4f^7$. Hence third-order terms (3b) with $V = H_{\mathrm{CF}}$, which allow $\Delta L, \Delta J \leq 6$, can and do[3] permit a relatively strong linkage of $^8S_{7/2}$ to ^6I_J. A further contribution comes from fourth-order terms[1] with $V = H_{\mathrm{CF}}$ and $V' = H_{\mathrm{so}}$, which allow $\Delta S = 1$ in addition, thus permitting a direct linkage of ^8S to ^6I.

The fully recoupled third and fourth operators which result following closure over the intermediate states of the $4f^6 5d$ configuration have been stated in I [expressions (6a) and (7)]. In applying these results to the Eu^{2+}:CaF_2 data shown in Fig. 6, three elementary changes are required.

(1) We must use the cubic crystal-field Hamiltonian (2) for the CaF_2 host. The coefficients $B_q^{(k)}$ now involve radial integrals of the $5d$ electron and are determined by the crystal-field splitting of $4f^6 5d$ levels,[7] which is dominated by the splitting of the ^2D level of the outer $5d$ electron into T_{2g} and E_g states separated by 17 000 cm^{-1}. Diagonalization of the Hamiltonian (2) yields a ^2D splitting of $\frac{1}{2}B_0^{(4)}$, yielding $B_0^{(4)} = 34\,000$ cm^{-1}. The sixth-rank crystal-field operators do not act upon the $5d$ electron, and the crystal interaction with the $4f^6$ core can be neglected.

(2) The spin-orbit parameter $\zeta = \zeta_f \simeq 2\zeta_d \simeq 1200$ cm^{-1} for Eu^{2+} must be used.

(3) The average energy denominator E_{df} is reduced by a factor of 3 or so compared to Gd^{3+}. In fact, the only active intermediate states are the octets and sextets, which lie at the lower edge of $4f^6 5d$ at an average energy of $E_{df} \simeq 35\,000$ cm^{-1} above an optical excitation energy.

Taking into account these differences, it is now a straightforward matter to compare the calculated ^6I_J intensities for Eu^{2+}:CaF_2 to those[1] for Gd^{3+}:LaF_3. The third-order contribution scales as $(B_0^{(4)}/E_{df})^2$, while the fourth-order contribution scales as $(B_0^{(4)}/E_{df})^2(\zeta/E_{df})^2$. For Eu^{2+}:CaF_2, we estimate $B_0^{(4)}/E_{df} \sim 1$ and $\zeta/E_{df} \sim 0.03$ in contrast to about 0.04 and 0.01, respectively, for Gd^{3+}:LaF_3. These ratios were adjusted slightly to fit the data in Fig. 6. The solid circles in this figure show the line strengths calculated using only the third-order contribution with $B_0^{(4)}/E_{df} = 1.25$. The circled crosses include both third- and fourth-order contributions with $B_0^{(4)}/E_{df} = 1.25$ and $\zeta/E_{df} = 0.03$. Evidently, the order-of-magnitude strengthening of these lines relative to $^6P_{5/2}$, ^6D_J is well explained with physically reasonable parameters, and constitutes strong evidence for the higher-order nature of the line intensities.

J mixing among the $4f^7$ levels has some additional influence on the line strengths, though much less than that in the corresponding Gd^{3+}:LaF_3 case. Analysis of that data[1] showed that the small admixture of $^6P_{7/2}$ in the ^6I_J

wave functions led to a new contribution to the line strengths which interfered with the above-mentioned contributions in a polarization-dependent fashion, resulting in a strong anisotropy. The lack of such strong anisotropy in the present data is a consequence of the higher substitution site symmetry (O_h) of CaF_2 compared to LaF_3 (D_{3h}). Crystal-field terms $B_4^{(4)}C_{\pm 4}^{(4)}$ are thus present in addition to $B_0^{(4)}C_0^{(4)}$, and give rise to third- and fourth-order operators of the form $O_q^{(6)}$, with $q \neq 0$, for all linear polarizations. The matrix elements of these operators do not interfere with the matrix elements of the principal operator acting on the $^6P_{7/2}$ admixture, which has the scalar form[6] $W_0^{(11)0}$ for linear polarization. Furthermore, the third- and fourth-order contributions to ^6I_J are much stronger in Eu^{2+}:CaF_2 than the contribution from the $^6P_{7/2}$ admixture, further decreasing the degree of interference between them. Strong mixing of excited-state azimuthal quantum numbers in the cubic field also tends to average out anisotropy. As a result, the effect of the $^6P_{7/2}$ admixtures in Eu^{2+}:CaF_2 is simply to enhance the calculated ^6I_J intensities by very small and nearly equal amounts for each linear polarization. Admixtures of other ^6P and ^6D levels into ^6I_J can be neglected, although mixing among the ^6I_J levels probably produces some additional anisotropy which has not been taken into account.

C. $^8S_{7/2} \rightarrow {}^6P_{7/2,5/2}, {}^6D_{7/2}$: Third-order terms involving the spin-orbit interaction

The third-order TPA operator with $V = H_{so}$ was first derived by Judd and Pooler,[6] and has been applied in I to a detailed analysis of the $^8S_{7/2} \rightarrow {}^6P_{7/2,5/2,3/2}, {}^6D_{7/2}$ transition intensities for Gd^{3+}:LaF_3. The most notable effect of this operator in Gd^{3+} was a nearly 100-fold enhancement of the $^6P_{7/2}$ intensity for linear polarization over the intensity predicted in second order. The presence of a similar enhancement in the Eu^{2+} data is incontrovertible evidence that the same third-order linkage is at work.

Nevertheless, this third-order contribution is much weaker than expected. It should scale as $(\zeta/E_{df})^2$, and thus increase by roughly an order of magnitude to the line strengths shown by crosses in Fig. 6. In each case where a sharp increase is expected, however, it is not observed.

We have examined[4] the effect of including intermediate configurations higher in energy than $4f^6 5d$, such as $4f^6 ng$, $4f^6 nd$, or $3d^9 4f^8$, upon the calculated intensities of $^6P_{7/2,5/2}, {}^6D_{7/2}$. Careful examination of the new third-order operators which come into play shows that they can only increase the predicted intensities of these lines. This fact, along with the large energy denominators of the higher configurations and the success of the Gd^{3+} analysis[1] based solely on $4f^6 5d$ intermediate states, are strong arguments that these higher configurations can be neglected for the transitions in question. In Sec. V E, therefore, we examine another possible source of the discrepancy.

D. $^8S_{7/2} \rightarrow {}^6D_{1/2}$

The intensity of the weak $^6D_{1/2}$ line, as in Gd^{3+}:LaF_3, can be explained by the admixture of $^6D_{7/2}$ present in the $^6D_{1/2}$ wave function. Using the approximate crystal-field parameter $B_0^{(4)} = -3300\ cm^{-1}$ obtained from the energy-level fit, we obtain the admixture

$$|\{{}^6D_{1/2}, \pm\tfrac{1}{2}\}) = 0.59\,|[{}^6D_{1/2}, \pm\tfrac{1}{2}]) + 0.38\,|[{}^6D_{7/2}, \pm\tfrac{1}{2}]) + 0.31\,|[{}^6D_{7/2}, \mp\tfrac{7}{2}])\ ,$$

where curly brackets around the term designation indicate that crystal-field mixing has been taken into account. We thus obtain the intensity ratios

$$S({}^6D_{7/2}, \vec{E}||[100]) = 20S({}^6D_{1/2}, \vec{E}||[111]), 16S({}^6D_{1/2}, \vec{E}||[100]), 15S({}^6D_{1/2}, \text{circular})\ ,$$

which agree acceptably well with the observed intensity ratios for these two lines shown in Fig. 6. Most importantly, the lack of strong anisotropy, which this line showed in Gd^{3+}:LaF_3, follows consistently from this explanation. The line is isotropic because in cubic symmetry the $M_J = \pm\frac{7}{2}$ component of $^6D_{7/2}$ is mixed into the $^6D_{1/2}$ wave function in addition to $M_J = \pm\frac{1}{2}$.

E. Validity of the closure approximation

We believe that a significant part of the discrepancy for $^6P_{7/2,5/2}, {}^6D_{7/2}$ results from a breakdown of the closure approximation for the divalent ion. Unfortunately, the computational task of summing over thousands of intermediate states usually becomes unmanageable if the closure approximation is relaxed. Since, however, the Coulomb interaction is primarily responsible for the spread of levels in the intermediate configurations, the computation of higher-order terms involving the Coulomb interaction among the intermediate states should account for the effects of breakdown of the closure approximation, even though allowing the use of closure as a computational tool. The evaluation of such new terms is, however, beyond the scope of the present paper.

Instead we adopt the more direct approach of introducing term-dependent energy denominators and performing the sum over intermediate states explicitly. We have found that for the case of the third-order contribution to $^8S_{7/2} \rightarrow {}^6P_{7/2}$ ($^6P_{5/2}$), only 42 (33) of the $(2725)^2$ possible third-order terms are nonvanishing for each M_J value of the excited state. Furthermore, some factors are common to all terms in the sum and need not be recomputed each time. The explicit sum thus reduces to manageable dimensions for this specific case.

Figure 7 illustrates the levels of $4f^6 5d$ which come into play in the third-order contribution to $^8S_{7/2} \rightarrow {}^6P_{7/2,5/2}$. The electric dipole operator (dotted line) links $f^7\ {}^8S_{7/2}$ to $f^6({}^7F)d\ {}^8P_J$. The spin-orbit operator (dashed line), which is diagonal in J and M_J, then links $f^6({}^7F)d\ {}^8P_J$ to numerous $^6S_{5/2}$, ^6P_J, and ^6D_J levels derived from various f^6 parent states. These in turn are linked to $^6P_{7/2}$ or $^6P_{5/2}$ by a second electric dipole operator. The energies of the

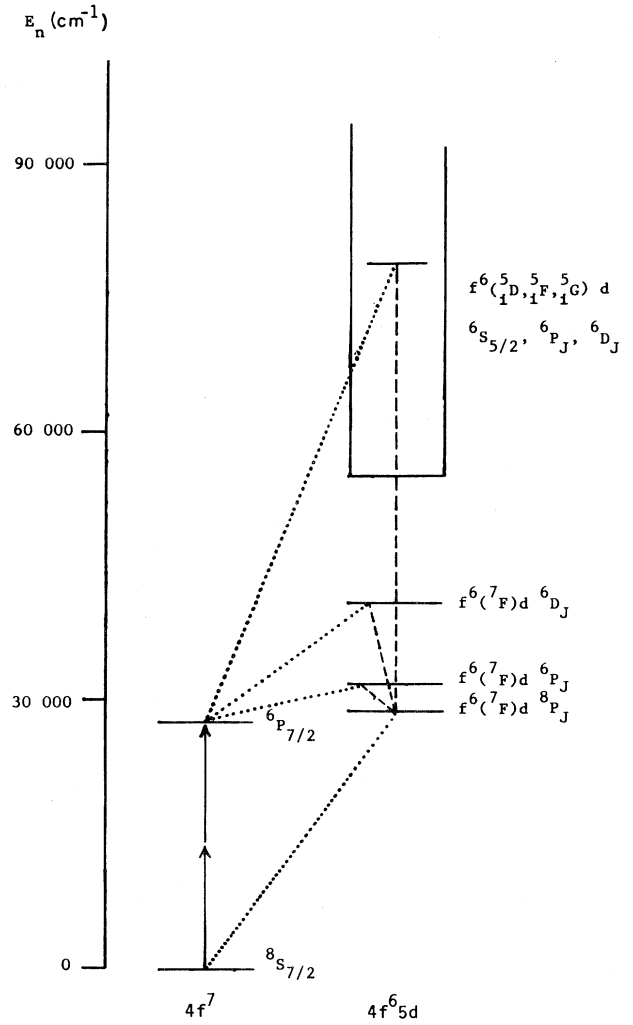

FIG. 7. Partial energy-level diagram of Eu^{2+} showing levels of the $4f^6 5d$ configuration which serve as intermediate states in the third-order contribution to the two-photon $^8S_{7/2} \rightarrow {}^6P_{7/2,5/2}$ transitions. Dotted lines denote interconfigurational electric dipole linkages, while the dashed lines denote spin-orbit linkages within $4f^6 5d$.

intermediate states were estimated from the free-ion spectrum[19] of Eu^{2+}, corrected for a nephelauxetic reduction of about 10 000 cm^{-1} in the crystal.

The third-order term to be evaluated is

$$E_0^{-1}E_i^{-1}(f^7\,{}^8S_{7/2} \mid \vec{E}\cdot\vec{D} \mid f^6 d\,{}^8P_J) \times (f^6 d\,{}^8P_J \mid H_{so} \mid f^6 di)(f^6 di \mid \vec{E}\cdot\vec{D} \mid f^7\,{}^6P_J)\,, \tag{4}$$

where E_0 is the energy of $f^6 d\,{}^8P_J$ above $h\nu$. The three matrix elements in each term can be evaluated by standard tensor operator techniques (see, for example, formulas 2-110 and 3-16 of Wybourne[28]). Table III shows the results of the computations. The intermediate states have been divided into three groups which have been assigned energy denominator E_1 [$f^6(^7F)d\,{}^6P_J$ states], E_2 [$f^6(^7F)d\,{}^6D_J$ states], and E_3 [the entire group of $f^6(^5D,{}^5F,{}^5G)d\,{}^6S_{5/2},{}^6P_J,{}^6D_J$ states]. The third-order term (4) has been computed for $^6P_{7/2}$ and $^6P_{5/2}$ final states for linearly and circularly polarized excitation. In each column the terms from each group of intermediate states, if given a common energy denominator, sum to the result obtained using the closure approximation.

Two important conclusions on the effect of relaxing the closure approximation can now be drawn from the results shown in Table III. Firstly, in all cases the ζ_d part of the operator arises entirely from the two lowest sets of sextet levels, namely $f^6(^7F)d\,{}^6P_J,{}^6D_J$. Consequently, the ζ_d part of the third-order operator is more heavily weighted than when an average energy denominator $E_{df} \simeq 40\,000$ cm^{-1} is used. Secondly, in all cases the ζ_f part of the operator arises almost entirely from the highest group of sextet levels, namely $f^6(^5D,{}^5F,{}^5G)d\,{}^6S_{5/2},{}^6P_J,{}^6D_J$. In fact, more detailed calculations show that for $^6P_{7/2}$ and linear polarization, about $\frac{2}{3}$ of the ζ_f part of the operator stems from the highest levels of this upper group, namely $f^6(^5F,{}^5G)d\,{}^6P_J,{}^6D_J$, which probably lie 70 000 to 100 000 cm^{-1} above the single photon energy. The energy denominator is thus 2 to 3 times larger than E_{df}, and consequently this part of the operator is less heavily weighted than with the average energy denominator.

The effect of distributing the weighting factors in this way is in all cases to decrease the predicted intensity contributed by the third-order operator in the spin-orbit interaction. By choosing the reasonable energy values $E_1 = 20\,000$, $E_2 = 30\,000$, and $E_3 = 67\,000$ cm^{-1}, along with the spin-orbit constants $\zeta_f = 2\zeta_d = 1200$ cm^{-1}, the third-order contribution for $^6P_{7/2}$, circular polarization, and $^6P_{5/2}$, all polarizations can be reduced to zero. In effect, the part of the third-order term proportional to ζ_f and the part proportional to ζ_d, which are opposite in sign, are made to cancel by this choice of energy denominators. On this supposition, the line strengths for $^6P_{7/2}$ with circular polarization and $^6P_{5/2}$ with all polarizations come from the second-order contribution alone. The data in Fig. 6 fully support this revision in the theoretical prediction.

For $^6P_{7/2}$, linear polarization, a similar cancellation does not occur. Nevertheless, the predicted intensity decreases by a factor of 4 to 5 when closure is relaxed, since the greatest part of the third-order contribution comes from the highest group of intermediate states. The same correction applies for $^6D_{7/2}$ with linear polarization, since here the third-order term contributes only because there is an admixture of $^6P_{7/2}$ into $^6D_{7/2}$ from the spin-orbit interaction.[1] In the latter case, the correction is nearly adequate to explain the data in Fig. 6, although for $^6P_{7/2}$ the correction is still too small to explain the relatively weak observed intensity. It is encouraging nevertheless to see that in all cases the corrections have been in the right direction.

For the other theoretical predictions shown in Fig. 6 the effect of relaxing the closure approximation is, unfortunately, much more difficult to estimate since a great many more terms enter the sum. Higher-order contribu-

TABLE III. Third-order contributions to the two-photon absorption intensities of $^8S_{7/2} \rightarrow {}^6P_{7/2,5/2},M$ for linear and circular polarization arising from each of three groups of intermediate states from the $4f^6 5d$ configuration. Third-order terms calculated by using the closure approximation and a single energy denominator E_{df} are shown for comparison.

Intermediate states	$^6P_{7/2},M$ $(\vec{E}\|\|\vec{z})$[a]	$^6P_{7/2},M$(circular)[a]	$^6P_{5/2},M$ $(\vec{E}\|\|\vec{z})$[a]	$^6P_{5/2},M$(circular)[a]
$f^6(^7F)d^6P_J$	$aE_1^{-1}[(\frac{1}{12}\zeta_f+\frac{1}{2}\zeta_d)+\alpha(M)(\frac{5}{6}\zeta_f+5\zeta_d)]$	$aE_1^{-1}\beta(M)(\frac{5}{6}\zeta_f+5\zeta_d)$	$-bE_1^{-1}\gamma(M)(\frac{5}{6}\zeta_f+5\zeta_d)$	$bE_1^{-1}\delta(M)(\frac{5}{6}\zeta+5\zeta_d)$
$f^6(^7F)d^6D_J$	$aE_2^{-1}[(\frac{1}{12}\zeta_f+\frac{1}{2}\zeta_d)-\alpha(M)(\frac{1}{6}\zeta_f+\zeta_d)]$	$-aE_2^{-1}\beta(M)(\frac{1}{6}\zeta_f+\zeta_d)$	$bE_2^{-1}\gamma(M)(\frac{1}{6}\zeta_f+\zeta_d)$	$-bE_2^{-1}\delta(M)(\frac{1}{6}\zeta_f+\zeta_d)$
$f^6(^5_iD,^5_iF,^5_iG)d^6S_{5/2},{}^6P_J,{}^6D_J$	$aE_3^{-1}[\frac{53}{6}\zeta_f-\alpha(M)\frac{29}{3}\zeta_f]$	$-aE_3^{-1}\beta(M)\frac{29}{3}\zeta_f$	$bE_3^{-1}\gamma(M)\frac{29}{3}\zeta_f$	$-bE_3^{-1}\delta(M)\frac{29}{3}\zeta_f$
Using closure:	$aE_{df}^{-1}[(9\zeta_f+\zeta_d)-\alpha(M)(9\zeta_f-4\zeta_d)]$	$-aE_{df}^{-1}\beta(M)(9\zeta_f-4\zeta_d)$	$bE_{df}^{-1}\gamma(M)(9\zeta_f-4\zeta_d)$	$-bE_{df}^{-1}\delta(M)(9\zeta_f-4\zeta_d)$

[a]Coefficients: $a=\frac{2}{3}(\frac{1}{14})^{1/2}E^2/E_0$,

$b=2(\frac{2}{105})^{1/2}E^2/E_0$,

$\alpha(M)=\frac{1}{140}(M^2-\frac{21}{4})$,

$\beta(M)=\frac{1}{280}[(\frac{5}{2}-M)(\frac{7}{2}-M)(\frac{9}{2}-M)(\frac{11}{12}+M)]^{1/2}$,

$\gamma(M)=M/140(\frac{49}{4}-M^2)^{1/2}$,

$\delta(M)=\frac{1}{280}[(\frac{5}{2}-M)(\frac{7}{2}+M)(\frac{9}{2}+M)(\frac{11}{2}+M)]^{1/2}$.

tions involving the crystal-field interaction are particularly unwieldy since the crystal-field operator, unlike the spin-orbit operator, is not diagonal in J. Computation of higher-order terms in the Coulomb interaction may, therefore, be the only practical way of predicting the effects of relaxing the closure approximation in these cases.

VI. CONCLUSION

The known spectrum of Eu^{2+} in crystals has been greatly expanded by using two-photon spectroscopy to observe sharp $4f^7$ levels which are not observable by one-photon absorption because of the overlapping $4f^6 5d$ configuration. Similar configuration overlap occurs in all the divalent lanthanides in crystals, as well as in many trivalent lanthanides above about 40 000 cm^{-1} and in actnides. Two-photon spectroscopy should therefore permit numerous $4f^N$ and $5f^N$ spectra to be observed and classified for the first time.

Accurate measurements of the relative intensities and polarization dependence of the $f^7 \rightarrow f^7$ transitions in Eu^{2+}:CaF_2 have permitted us to test the applicability of line-strength theory developed[1] for Gd^{3+} to the corresponding divalent ion. The importance of third- and fourth-order contributions to the two-photon intensity which involve spin-orbit and/or crystal-field interactions among the intermediate states has been confirmed, although such contributions were substantially weaker than expected in some cases. An illustrative calculation showed that relaxing the closure approximation sharply affected some predicted intensities, and improved the overall agreement with the experimental results. Further theoretical work will be required, however, to account for a breakdown of the closure approximation in a fully consistent fashion.

ACKNOWLEDGMENTS

The advice, encouragement, and inspiration provided by Professor N. Bloembergen throughout the course of this research is gratefully acknowledged. M.C.D. thanks Professor Brian Judd for valuable discussions. This research was supported by the Joint Services Electronics Program under Contract No. N00014-75-C-0648.

*Present address: Bell Laboratories 4D515, Holmdel, NJ 07733.
†On leave from Departamento de Matemática y Física, Colegio Universitario de Cayey, Cayey, Puerto Rico.

[1] M. C. Downer and A. Bivas, Phys. Rev. B 28, 3677 (1983).
[2] M. Dagenais, M. Downer, R. Neumann, and N. Bloembergen, Phys. Rev. Lett. 46, 561 (1981).
[3] M. C. Downer, A. Bivas, and N. Bloembergen, Opt. Commun. 41, 335 (1982).
[4] M. C. Downer, Ph.D. thesis, Harvard University, Cambridge, 1983 (unpublished).
[5] J. D. Axe, Jr., Phys. Rev. 136, A42 (1964).
[6] B. R. Judd and D. R. Pooler, J. Phys. C 15, 591 (1982).
[7] E. Loh, Phys. Rev. 184, 348 (1969).
[8] U. Fritzler and G. Schaak, J. Phys. C 9, L23 (1976).
[9] U. Fritzler, Z. Phys. B 27, 289 (1977).
[10] S. N. Bodrug, E. G. Valyashko, V. N. Mednikova, D. T. Sviridov, and R. K. Sviridov, Opt. Spektrosk. 34, 312 (1973) [Opt. Spectrosc. 34, 176 (1973)].
[11] F. M. Ryan, M. Lehmann, D. W. Feldmann, and J. Murphy, J. Electrochem. Soc. 121, 1475 (1974).
[12] M. V. Hoffman, J. Electrochem. Soc. 119, 905 (1972).
[13] M. Inoue and Y. Toyazawa, J. Phys. Soc. Jpn. 20, 363 (1965).
[14] T. R. Bader and A. Gold, Phys. Rev. 171, 997 (1968).
[15] E. Bayer and G. Schaak, Phys. Status Solidi 41, 827 (1970).
[16] Z. J. Kiss and P. N. Yocum, J. Chem. Phys. 41, 1511 (1964).
[17] J. Makovsky, J. Chem. Phys. 46, 390 (1967).
[18] G. H. Dieke, *Spectra and Energy Levels of Rare Earth Ions in Crystals* (Wiley, New York, 1968).
[19] J. Sugar and N. Spector, J. Opt. Soc. Am. 64, 1484 (1974).
[20] (a) J. M. O'Hare and V. L. Donlan, Phys. Rev. 185, 416 (1969); (b) W. T. Carnall, H. Crosswhite, H. M. Crosswhite, and J. G. Conway, J. Chem. Phys. 64, 3582 (1976).
[21] W. T. Carnall, H. Crosswhite, and H. M. Crosswhite (unpublished), of Argonne National Laboratory, have made a compilation of energy level structure and transition probabilities in the spectra of trivalent lanthanides in LaF_3. Copies of this unpublished compilation are available from its authors upon request.
[22] J. C. Slater, Phys. Rev. 34, 1293 (1929).
[23] K. Rajnak and B. G. Wybourne, Phys. Rev. 132, 280 (1963).
[24] B. R. Judd, Phys. Rev. 141, 4 (1966).
[25] K. Rajnak and B. G. Wybourne, Phys. Rev. 134, A596 (1964).
[26] B. R. Judd, H. M. Crosswhite, and H. Crosswhite, Phys. Rev. 169, 130 (1968).
[27] K. H. Hellwege, Ann. Phys. (Leipzig) 4, 95 (1949).
[28] B. G. Wybourne, *Spectroscopic Properties of Rare Earths* (Wiley, New York, 1965).